Available online at www.sciencedirect.com
ScienceDirect
Surface & Coatings Technology 201 (2007) 4505–4511
SURFACE & COATINGS TECHNOLOGY
www.elsevier.com/locate/surfcoat

Oxidation tuning in AlCrN coatings

J.L. Endrino [a], G.S. Fox-Rabinovich [b,*], A. Reiter [a], S.V. Veldhuis [b], R. Escobar Galindo [c], J.M. Albella [c], J.F. Marco [d]

[a] Balzers AG, General Coating, FL-9496 Balzers, Principality of Liechtenstein
[b] Department of Mechanical Engineering, McMaster University, Ontario, Canada L8S 4L7
[c] Instituto de Materiales de Madrid, C.S.I.C., Cantoblanco, 28049 Madrid, Spain
[d] Instituto de Química-Física "Rocasolano" C.S.I.C., 28006 Madrid, Spain

Received 14 March 2006; accepted in revised form 11 September 2006
Available online 27 October 2006

Abstract

In this work, we have studied the influence of the coating design and composition on the oxidation behavior of $Al_xCr_{1-x}N$ ($x=0.70$) coatings. In particular, we have studied the effect brought about by the deposition of an additional subsurface titanium nitride barrier layer as well as by the doping of the AlCrN-based coatings by tungsten, boron and silicon. The coatings studied have been deposited using the cathodic arc vacuum (CAV) technique. The multilayered AlCrN/TiN coatings with TiN sublayer were oxidized in air at 900 °C over 3 h and then analyzed by Glow Discharge Optical Emission Spectroscopy (GDOES) and X-ray photoelectron spectroscopy (XPS). Oxidation tests were performed in air at 900 and 1100 °C for the AlCrN and AlCrWN, AlCrSiN, and AlCrBN coatings. In each case weight gain was measured and the surface morphology of the oxidized samples were studied using Secondary Electron Microscopy (SEM) and Energy Dispersive Spectroscopy (EDS). The results obtained showed that the oxidation behavior of the aluminum rich AlCrN-based coatings could be improved in two ways: (1) by controlling the chromium outward diffusion rate in multi-layered coatings and (2) by alloying the AlCrN-based coatings with Si. Both improvements are related to the enhancement of the protective oxide film formation.

Keywords: Arc evaporation; Nitrides; Oxidation resistance; Glow Discharge Optical Emission Spectroscopy

1. Introduction

Chromium nitride coatings oxidize due to the outward diffusion of chromium and the formation of chromium oxide surface layers [1]. Oxidation studies have shown the superior oxidation resistance of the ternary $Al_xCr_{1-x}N$ as compared to $Al_xTi_{1-x}N$ [1–4]. This makes wear resistant $Al_xCr_{1-x}N$ coatings better candidates for many specific applications [1]. Recently, a number of studies have been performed on the impact of aluminum content on the hardness and oxidation resistance of Al–Cr–N coatings [2–4]. It has been reported that the hardness, oxidation resistance and the tribological properties improve with increasing Al-content up to 70–75% in the AlCrN coatings as long as the fcc-structure is predominant. For higher

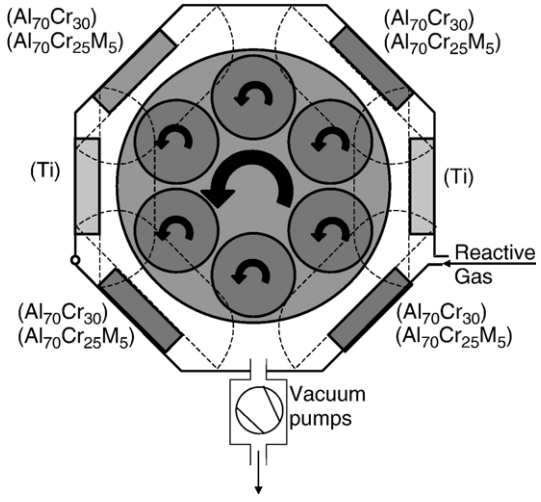

Fig. 1. Schematic illustration of the deposition chamber used for film deposition.

* Corresponding author. Tel.: +1 905 5259140x23127; fax: +1 905 521 2773.
E-mail address: gfox@mcmaster.ca (G.S. Fox-Rabinovich).

0257-8972/$ - see front matter © 2006 Elsevier B.V. All rights reserved.
doi:10.1016/j.surfcoat.2006.09.089

Table 1
Summary of deposition parameters

Targets composition	Ti, $Al_{70}Cr_{30}$, $Al_{70}Cr_{25}W_5$, $Al_{70}Cr_{25}B_5$, $Al_{70}Cr_{25}Si_5$
Targets power	$Al_{70}Cr_{25}M_5$(3.5 kW)–Ti(2.4 kW)
Nitrogen deposition pressure	3.5 Pa
Substrate materials	WC–6%Co inserts, Cold work tool steel disks, TiAl squares
Substrate bias voltage	−100 V
Substrate temperature	450 °C

aluminum content hcp-structure starts to form and the oxidation resistance deteriorates. In the hcp case the oxidation rate is almost tripled compared to the fcc-AlCrN.

The Al content in the AlCrN coatings is limited due to the undesirable phase transformation from B1 (cubic) to B4 (hexagonal) in the coatings with higher Al content. In general, the Cr and Al oxide films that are forming on the surface at high temperatures are expected to be the thermal barrier as well as the lubricating layers [5]. High aluminum content AlCrN coatings exhibit high short-term oxidation resistance up to 1100 °C due to the formation of alumina surface layers. However, after a longer exposure in air the surface layers become partially depleted of aluminum because intensive diffusion of Cr to the surface takes place which results in the formation of Cr_2O_3. In some cases complex $(Al, Cr)_2O_3$ oxide films are formed due to the solubility of Cr_2O_3 in alumina [6]. Since oxidation is interrelated with the inward diffusion of oxygen into the surface of the AlCrN coating and the outward diffusion of Cr to the surface, it is believed that the oxidation behavior of the aluminum-rich AlCrN coatings can be tuned by the design and composition of the coating. In the present study, we investigate the influence of buried TiN diffusion barrier layers as well as the addition of W, B, and Si on the oxidation resistance of $Al_{0.70}Cr_{0.30}N$-based coatings.

2. Experimental

In the present study, a front-loading Balzers' rapid coating system (RCS) machine was used for the deposition of the coatings. This system is shown schematically in Fig. 1. The machine is equipped with 6 cathodic arc sources. Two of the six sources were used to deposit a thin, 0.3 μm thick titanium nitride sub-layer to improve adhesion of all the coatings. The remaining four sources were employed to deposit the main layer of the coatings, which was obtained using customized sintered targets.

Table 2
Characterization data for coatings with intermediate titanium nitride layers

Coating #	Total thickness (μm)	Buried depth of TiN (μm)
1 – TiN at the surface	3.2	0.5
2	3.2	0.7
3	3.1	1.1
4	3.3	1.4
5	3.3	1.7
6	3.3	2
7	3.2	2.3
8 – TiN at the substrate	3.0	2.8

Table 3
Chemical characterization data for AlCrMN coatings (EDX and Electron Probe Microanalysis data)

Coating	Cr/Al	M/Al
AlCrN	0.55	–
AlCrWN	0.49	0.08
AlCrBN [a]	0.51	0.04
AlCrSiN	0.48	0.08

[a] Content measured by electron probe microanalysis.

The compositions of the targets used are shown in Table 1. During the deposition, the chamber was back filled with pure reactive nitrogen to a pressure of 3.5 Pa and the temperature of the substrates was held at approximately 450 °C. Also, a bias voltage of −100 V was applied to the substrates. A set of eight samples with AlCrN multi-layered coatings containing intermediate TiN layers was prepared using titanium (Ti) and $Al_{70}Cr_{30}$ targets. Table 2 shows the total coating thickness and the depth of the titanium nitride (TiN) buried layer for all the samples. The samples were annealed in air for 3 h at 900 °C. In addition to the AlCrN/TiN multi-layered coatings, the quaternary nitride AlCrWN, AlCrBN and AlCrSiN coatings were prepared by

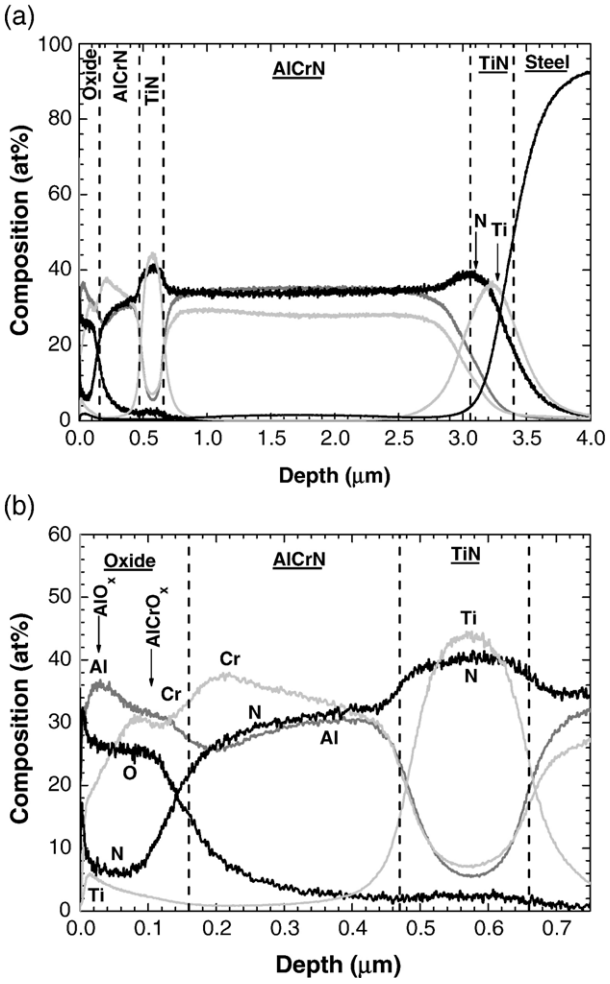

Fig. 2. Glow Discharge Optical Emission Spectroscopy depth-profiles of sample #1 (TiN layer near the surface) oxidized at 900 °C for 3 h: (a) general scan, (b) oxidized layer.

cathodic arc evaporation from $Al_{70}Cr_{25}W_5$, $Al_{70}Cr_{25}B_5$, and $Al_{70}Cr_{25}Si_5$ targets to study the impact of tungsten, boron, and silicon addition on the oxidation behavior of high-aluminum content AlCrN-based coatings [7–10]. It was shown earlier that AlCrN-based coatings can also have cubic B1 crystal structure [10]. The chemical composition of the binary and ternary coatings is presented in Table 3 (EDS and Electron Probe Microanalysis data). All the AlCrN coatings were deposited on all the sides of square 13×13 mm mirror polished cemented carbide (WC–6% Co) substrates; 20×20 mm square γ-TiAl samples, and 20 mm-diameter cold work tool steel samples.

Glow Discharge Optical Emission Spectroscopy (GDOES) [11,12] depth profile analysis of the coatings on the steel substrate was completed using a Jobin Yvon RF GD Profiler equipped with a 4 mm diameter anode and operating at a typical radio frequency discharge pressure of 650 Pa and power of 40 W. Quantified profiles were obtained automatically using the standard Jobin Yvon QUANTUM Intelligent Quantification software. The setup was calibrated using standard materials of known composition. In the quantification of nitrogen, we used a series of chromium nitride coatings with atomic content of nitrogen up to 40%. The composition of these homemade standards was measured by means of Rutherford Backscattering Spectroscopy.

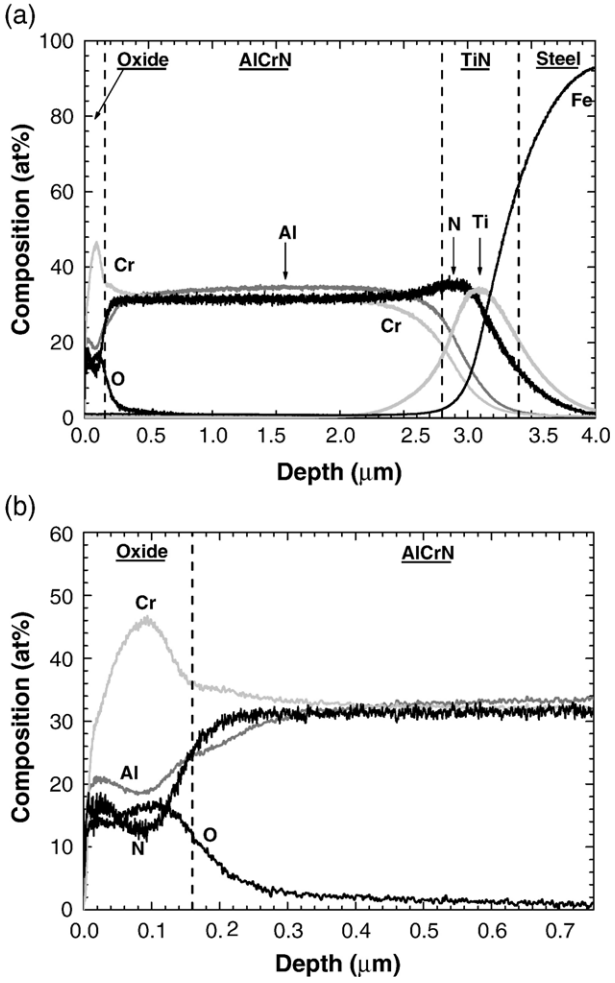

Fig. 3. Glow Discharge Optical Emission Spectroscopy depth-profiles of sample #8 (no intermediate TiN layer) oxidized at 900 °C for 3 h: (a) general scan, (b) oxidized layer.

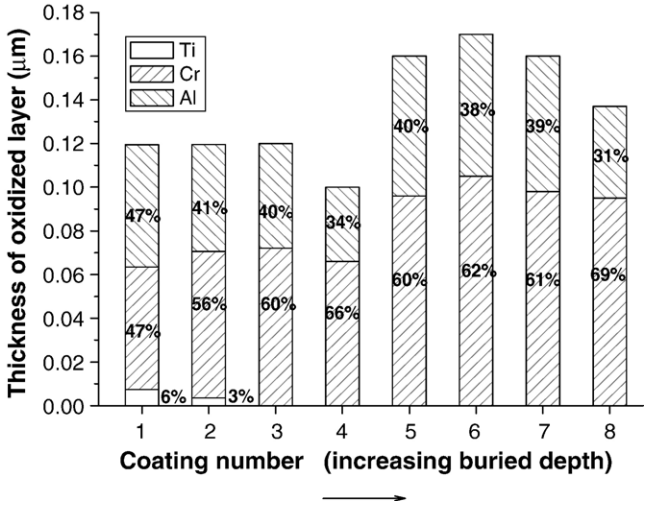

Fig. 4. Average Ti, Al, and Cr content in the oxidized layer for samples #1–#8 according to GDOES depth profile.

X-Ray photoelectron spectroscopy (XPS) data of an as-deposited AlCrN coating and of high temperature treated samples containing a TiN barrier layer were recorded with a triple channeltron CLAM2 analyzer using Al Kα radiation and a

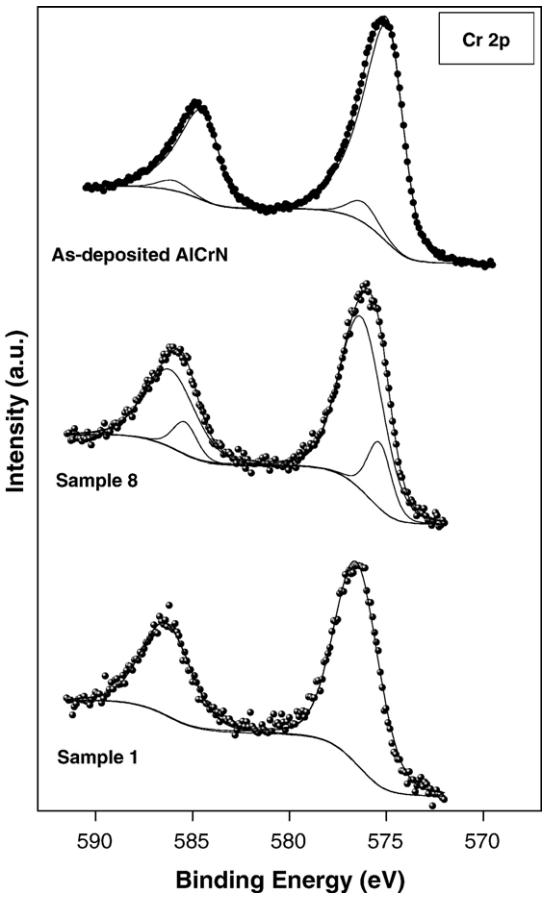

Fig. 5. Cr 2p spectra recorded from the as-deposited AlCrN coating, sample 8 and sample 1.

Table 4
Binding energies of the different species

Sample	Peak	E_B (eV)	Assignment	Reference
As-deposited AlCrN	Cr $2p_{3/2}$	575.2	Cr–N bonds in AlCrN	[13]
	Cr $2p_{3/2}$	576.3	Cr_2O_3	[15]
	N 1s	396.2	Metal–N bonds	[15]
	N 1s	398.0	Oxynitrides	[15]
	Al 2p	72.6	Al–N bonds	[13], this work
	Al 2p/Cr 3s	73.6 eV	Al–O bonds and/or Cr–N bonds	[16], this work
	Cr 3s	77.3 eV	Cr–N bonds in AlCrN	This work
# 1	Cr $2p_{3/2}$	576.3	Cr_2O_3	[15]
	N 1s	397.8	oxynitrides	[15]
	N 1s	399.9	oxynitrides	[15]
	Al 2p	73.1	N–Al–O bonds	This work
	Al 2p	74.3	Al_2O_3	[16]
# 8	Cr $2p_{3/2}$	575.3	Cr–N bonds in AlCrN	[13]
	Cr $2p_{3/2}$	576.3	Cr_2O_3	[15]
	N 1s	398.0	oxynitrides	[15]
	N 1s	399.8	oxynitrides	[15]
	Al 2p	72.6	Al–N bonds	[13], this work
	Al 2p/Cr 3s	73.8	Al–O bonds and/or other chromium species	[16], this work

constant analyzer transmission energy of 20 eV. All the spectra were recorded at take-off angles of 90°. Base pressure in the analysis chamber was typically around $6{\cdot}10^{-9}$ mbar. All binding energies (BE) were referred to the C 1s signal of the adventitious contamination carbon layer that was set at 284.6 eV. The BE's are accurate to ±0.2 eV.

Isothermal oxidation tests were performed in air, at 900 and 1100 °C during 1 and 3 h. Each specimen was placed in an alumina crucible. A lid was placed on the crucible immediately to recover spalled scales. The weight gain of the coated TiAl samples was measured. LEO 1530 scanning electron microscope (SEM) was used to study morphology of the oxidized specimens. EDS spectra have been obtained to measure chemical composition of the coating before and after oxidation. The Boron content in AlCrBN was determined using a CAMECA SX50 electron microprobe instrument.

3. Results

3.1. AlCrN multi-layered coatings with the subsurface TiN barrier layers

3.1.1. Glow discharge optical emission spectroscopy

The depth profile for the oxidized sample #1 (TiN buried depth: 0.5 μm) is shown in Fig. 2a. The profile indicates in this case that the outward diffusion of Cr to the outer surface starts below TiN layer. This demonstrates effectiveness of TiN as a diffusion barrier diffusion barrier for Cr within the AlCrN coating. The detailed GDOES profile from the oxidized surface of sample #1 (TiN near the surface) is shown in Fig. 2b. In this case, the depth profile shows the formation of a 50 nm Al-rich oxide film on the most outer surface. Titanium also was a part of the oxidized layer and reached a maximum concentration around ~8 at.% at the outer layer. The outward diffusion of the titanium seems to be a result of the close proximity of the TiN barrier layer, which is located only 0.5 μm deep from the outer surface of the coating. The AlO_x layer is followed by a 100 nm complex $AlCrO_x$ film, the average content of oxygen in the oxidized layer is around ~25 at.%. Fig. 3a, shows the GDOES depth profile for sample #8 (TiN near the substrate) after oxidation in air. The 2.5 μm thick $Al_{0.7}Cr_{0.3}N$ coating contains a complex 150 nm thick oxynitride layer at the surface. The detailed GDOES profiles from the surface (Fig. 3b) shows the formation of a film containing Al, O and N on the outer surface with the thickness around 50 nm. Intensive Cr and O pileups indicate the onset formation of a thick Cr-rich oxide layer below the Al–O–N outer film. A relatively low amount of oxygen (~15 at.%) detected in this layer can be related either to the presence of nitrogen, which inter-diffuses with oxygen or to a partial oxidation of the Cr diffusing from the coating. The relative content of Ti, Al and Cr (at.%) in the oxidized layer for all the eight deposited AlCrN/TiN multi-layered coatings are summarized in Fig. 4. The data presented shows that the oxidation behavior is mainly related to the buried depth of the TiN diffusion barrier layer. Indeed, samples #1–#4 (that contain a TiN layer near the surface) have substantially higher oxidation resistance than samples #5–#8, which had a TiN layer closer to the substrate. Also, the presence of the TiN layer near the outer surface most probably promotes the formation of Al-rich oxides and oxynitrides due to the limited supply of Cr atoms to the surface.

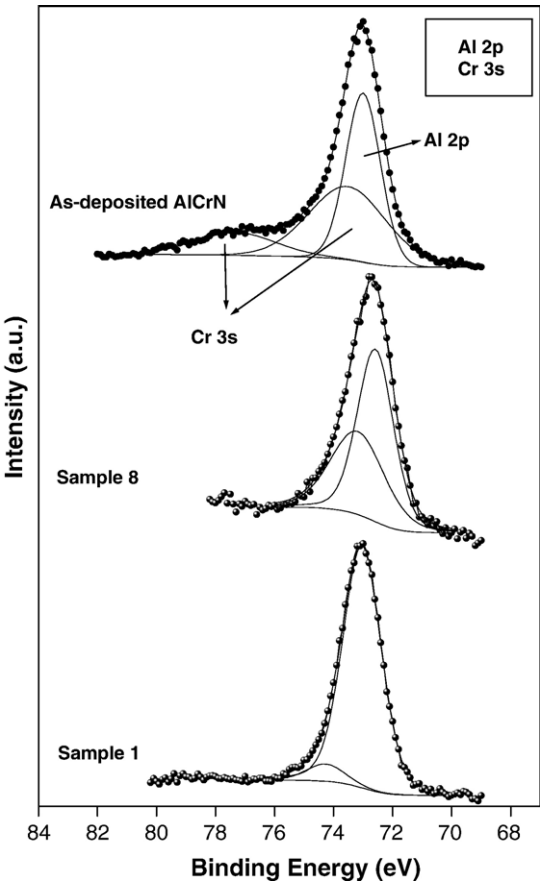

Fig. 6. Al 2p spectra recorded from the as-deposited AlCrN coating, sample 8 and sample 1.

3.1.2. X-ray photoelectron spectroscopy

The oxidation states of the elements within the outer oxidized layer (3–5 nm) were analyzed by XPS for the as-deposited AlCrN coating before the high temperature treatment as well as for sample #1 (TiN buried depth: 0.5 μm) and sample #8 (TiN layer near the substrate). The Cr 2p spectra recorded from these three samples are depicted in Fig. 5. The Cr 2p spectrum recorded from the as-deposited AlCrN film was best-fitted considering a main Cr 2p spin orbit doublet characterized by a binding energy of the Cr $2p_{3/2}$ level of 575.2 eV which we associate with the presence of Cr–N bonds [13,14] and a minor spin orbit doublet characterized by a binding energy of the Cr $2p_{3/2}$ level of 576.3 eV. This latter binding energy has been usually associated with the presence of Cr_2O_3 [15]. The Cr 2p spectrum recorded from sample #8 (TiN near the substrate) was also best-fitted considering two spin orbit doublets but, in this case, the minor one is characterized by a binding energy of the Cr $2p_{3/2}$ level of 575.3 eV and must correspond to Cr–N bonds as in the as-deposited AlCrN coating. The major one, characterized by a binding energy of the Cr $2p_{3/2}$ level of 576.3 eV, must correspond to the presence of Cr_2O_3. The Cr 2p spectrum recorded from sample #1 (TiN buried depth: 0.5 μm) was best fitted considering only one spin-orbit doublet characteristic of Cr_2O_3 [15]. Table 4 collects the corresponding binding energies for each component. The results indicate that, at least within the depth, which can be probed by XPS (ca. 3–5 nm), chromium is oxidized to Cr^{3+} as a consequence of the oxidation treatment and that the extent of chromium oxidation is higher in sample #1 than in sample #8.

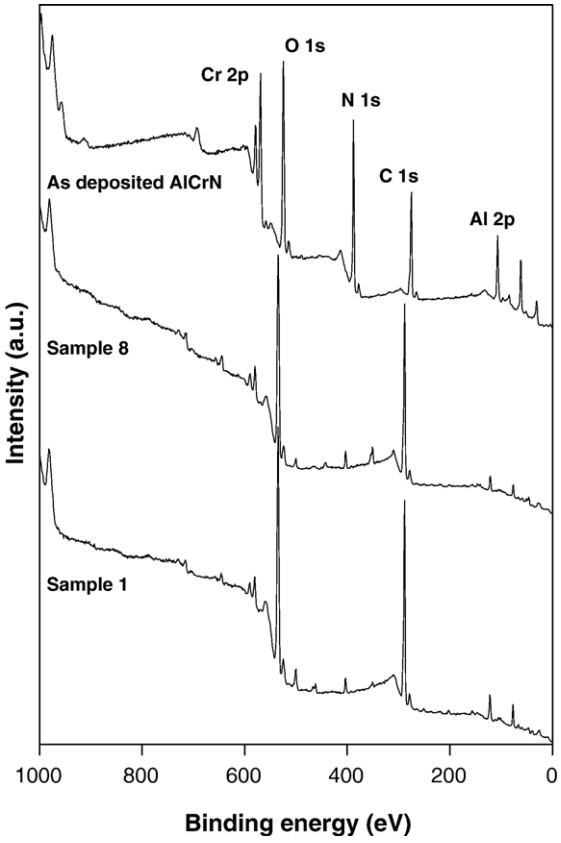

Fig. 7. Wide scan XPS spectra recorded from the as-deposited AlCrN coating, sample 8 and sample 1.

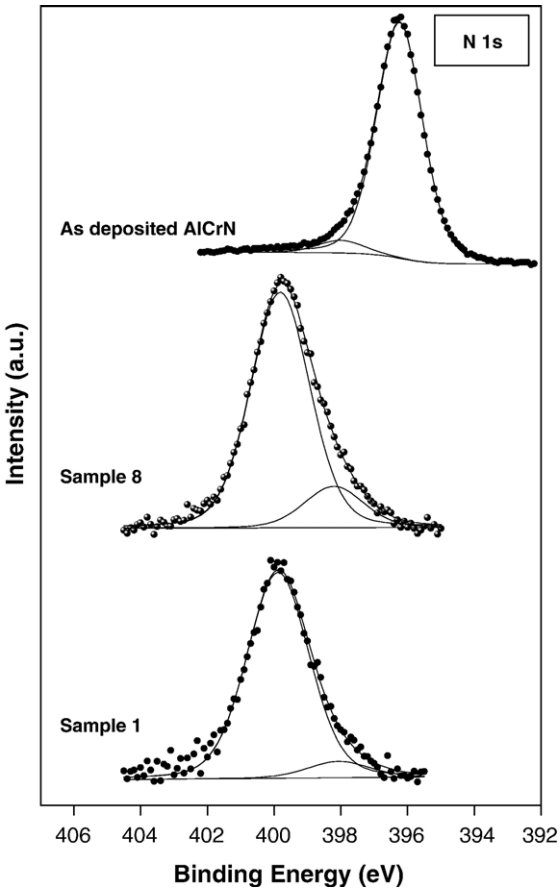

Fig. 8. N 1s spectra recorded from the as-deposited AlCrN coating, sample 8 and sample 1.

The Al 2p spectra recorded from the as deposited AlCrN coating and from samples #1 (TiN buried depth: 0.5 μm) and #8 (TiN layer near the substrate) are presented in Fig. 6. The Al 2p spectrum recorded from the as-deposited coating is dominated by a main contribution at 72.6 eV (Table 4), which we associate with the presence of Al–N bonds in the AlCrN film [13]. There is a strong overlap between the Al 2p peaks and the Cr 3s peaks appearing at 73.6 eV and 77.2 eV (the assignment of the peaks appearing at these energies as due to the Cr 3s core level was confirmed by recording the XPS spectrum of a pure CrN film). This makes difficult to discern if there are any other contributions

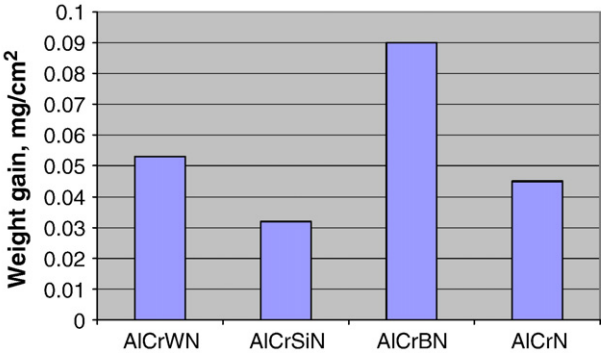

Fig. 9. Weight gain for AlCrN, AlCrWN, AlCrBN, and AlCrSiN samples after oxidation in air during 1 h at 900 °C.

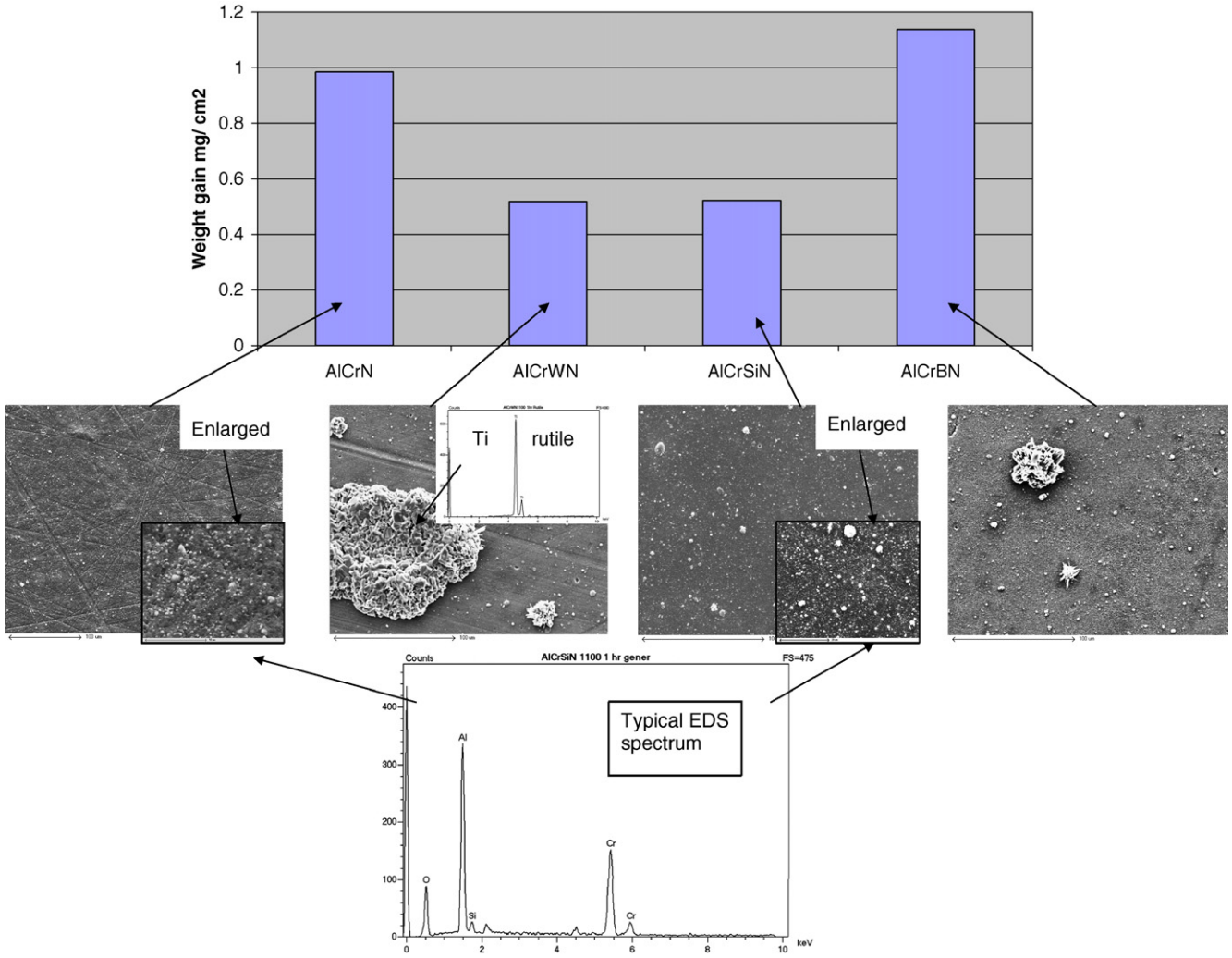

Fig. 10. Weight gain for AlCrN, AlCrWN, AlCrBN, and AlCrSiN samples after oxidation in air during 1 h at 1100 °C with SEM images of surface morphology.

corresponding to Al–O or N–Al–O bonds in this sample. A similar comment can be made concerning the Al 2p spectrum recorded from sample #8 (TiN near the substrate). However, the binding energy of the main component in the Al 2p spectrum recorded from the sample #1(TiN buried depth: 0.5 μm) is 73.1 eV (Table 4) that is, 0.5 eV higher than that found in the sample #8 and this might be related to the presence of N–Al–O bonds. We must take into account that, as a consequence of the oxidation treatment, the area of the Cr 2p peaks relative to that of the Al 2p peaks has decreased significantly in this sample, (Al/Cr area ratio = 4.17, see Fig. 7) respect to that observed in the as-deposited AlCrN film (Al/Cr area ratio = 5.26). Consequently, the intensity of the Cr 3s peaks has experienced also a large decrease, such that the above-mentioned overlap is almost insignificant in this sample (this is mainly evidenced by the absence of the Cr 3s peak which should appear at 77.3 eV in the corresponding spectrum, see Fig. 6). Therefore, the minor component appearing at 74.3 eV, and necessary to obtain a satisfactory fit of the spectrum, might be associated to the presence of Al_2O_3 [14,16].

The N 1s spectra recorded from the as deposited AlCrN coating and from samples #1 and #8 were also recorded (Fig. 8). The spectrum recorded form the as-deposited coating is dominated by a main component at 396.2 eV (Table 3), which we associate with the presence of nitride species [13]. The spectrum also shows a minor component at 398.0 eV, which we associate with the presence of oxynitrides [15]. The N 1s spectra recorded from samples #8 and #1 are quite different since they are dominated by a main contribution at 399.8 eV, which might correspond to N–Cr–O or N–Al–O bonds [15] (Table 4). They also contain a minor component at ca. 398.0 eV. The results indicate that the N species present in the original sample have suffered a significant oxidation after treatment at high temperature.

3.2. Ternary nitride AlCrWN, AlCrBN, and AlCrSiN coatings

The chemical composition of the deposited alloyed-AlCrN coatings is presented in Table 3 (EDS and Electron Probe

Table 5
Weight gain data for γ-TiAl substrates after oxidation in air at 900 and 1100 °C, during 1 h

Substrate material	Temperature, °C	Weight gain, mg/cm^2
γ-TiAl	900	0.371
	1100	9.6

Microanalysis data). Figs. 9 and 10 show the weight gain per unit area (mg/cm^2) for AlCrN-based quaternary nitride coatings deposited on γ-TiAl substrates after 1 h annealing in air at 900° and 1100 °C respectively. To present oxidation protection behavior of the physical (PVD) coatings the weight gain data for the un-coated γ-TiAl substrates is shown in Table 5. As it can be seen from Table 5 and Figs. 9–10 the deposited coatings significantly improve the oxidation resistance of the TiAl substrate. At the lower oxidation temperature of 900 °C the AlCrWN and AlCrBN samples show lower oxidation stability than the AlCrN coating. This is a result of the affinity of W to oxidation and of the probable formation of a liquid oxide phase during the oxidation of B-containing coatings [10,17]. The best short-term oxidation resistance was exhibited by the AlCrSiN coating most probably due to significant grain size refinement [18]. Coating with a finer grain size has enhanced aluminum and chromium outward diffusion that leads to protective oxide layers formation [19–21]. At higher temperatures of oxidation (1100 °C) AlCrSiN coatings show promising oxidation resistance.

Surface morphology investigation of the oxidized samples with AlCrWN, AlCrBN coatings by means of SEM indicates the formation of rutile agglomerates. Fig. 10 shows the distribution of rutile particles on the surface of the AlCrWN, AlCrBN sample. The EDS analysis of the surface oxide films also indicates the formation of rutile particles on the surface of the coatings. The rutile particles are formed due to the low protective ability of the ternary nitride coatings and oxidation of the γ-TiAl substrates. In contrast, the observations of the surface of the AlCrSiN coatings after oxidation (Fig. 10) revealed the formation of a continuous protective alumina or alumina/chromia oxide layer as discussed in Section 3.1. This layer efficiently protects the surface and prevents inward oxygen diffusion that results in the formation of rutile oxides. This implies that Al, Cr and Si probably work in synergy in the $Al_{70}Cr_{30}N$-based coating during short-term oxidation in air. Thus, this coating looks promising for oxidation protection at elevated temperatures. This result confirms the oxidation stability of the silicon-containing quaternary nitride coatings even for low amounts of silicon addition.

4. Conclusions

Chromium based hard coatings such as CrN and $Al_xCr_{1-x}N$ have been successfully applied as protective layers for stamping and forging tools due to their capacity to redirect the heat generating at the tool/workpiece interface. Today, hard aluminum chromium nitride coatings are replacing the titanium nitride-based hard coatings for many machining applications including milling and drilling operations. This is mainly possible due to the superior hot hardness and oxidation resistance of the $Al_xCr_{1-x}N$ coatings as compared to the $Al_xTi_{1-x}N$ ones. On the basis of the oxidation experiments presented in this work, modified aluminum-rich AlCrN-based coatings can change their oxidation behavior, because the formation of the oxide and oxynitride surface films is controlled by the outward diffusion of Cr and Al to the surface. Consequently, the oxidation behavior of the AlCrN-based coatings is tunable. In this paper, we have described two mechanisms in which a protective alumina layer can be formed: (i) by the presence of diffusion barrier layers near the surface of the coating. (ii) by means of synergistic alloying of the AlCrN-based coating with small amounts of Silicon.

Acknowledgements

This research was partially funded by the National Science and Engineering Research Council of Canada (Strategic Grant Project" Oxidation and protection of Ti and TiAl-based alloys for aerospace applications" and by the Spanish Ministry of Education (Projects no. no.MAT2005-05669-C03-02 and MAT2004-01451).

References

[1] J.E. Krzanowski, S.N. Basu, J. Patscheider, Y. Gogotsi (Eds.), Fall MRS Proceeding, vol. 843, 2005, p. 15, Boston.
[2] O. Banakh, P.E. Schmid, R. Sanjinés, F. Lévy, Surf. Coat. Technol. 163–164 (2003) 57.
[3] B. Mishra, C. Yamauchi (Eds.), TMS Annual Meeting, vol. 2, 2000, p. 291, Nashville.
[4] M. Hirai, Y. Ueno, T. Suzuki, W. Jiang, C. Grigoriu, K. Yatsui, J. Appl. Phys. 40 (2001) 1056.
[5] G.S. Fox-Rabinovich, K. Yamomoto, S.C. Veldhuis, A.I. Kovalev, G.K. Dosbaeva, Surf. Coat. Technol. 200 (2005) 1804.
[6] G.S. Fox-Rabinovich, G.C. Weatherley, A.I. Dodonov, A.I. Kovalev, L.S. Schuster, S.C. Veldhuis, G.K. Dosbaeva, Surf. Coat. Technol 177–178 (2004) 800.
[7] A.E. Reiter, V.H. Derflinger, B. Hanselmann, T. Bachmann, B. Sartory, Surf. Coat. Technol. 200 (2005) 2114.
[8] J.L. Endrino, G.S. Fox-Rabinovich, C. Gey, Surf. Coat. Technol. 200 (2006) 6840.
[9] W. Kalss, A. Reiter, V. Derflinger, C. Gey, J.L. Endrino, Int. J. Refract. Met. Hard Mater. 24 (2006) 399.
[10] G.S. Fox-Rabinovich, K. Yamomoto, S.C. Veldhuis, A.I. Kovalev, G.K. Shuster, L.S. Ning, Surf. Coat. Technol. 201 (2006) 1852.
[11] R. Payling, D. Jones, A. Bengtson, Glow discharge optical emission spectrometry, John Wiley and Sons, 1997.
[12] R. Winchester, R. Payling, Spectrochim. Acta, B 59 (2004) 607.
[13] R. Sanjinés, O. Banakh, C. Rojas, P.E. Schmid, F. Lévy, Thin Solid Films 420–421 (2002) 312.
[14] I. Bertóti, Surf. Coat. Technol. 151–152 (2002) 194.
[15] I. Milosev, H.-H. Strehblow, B. Navinsek, Thin Solid Films 303 (1997) 246.
[16] C.D. Wagner, D.E. Passoja, H.F. Hillery, T.G. Kinisky, H.A. Six, W.T. Jansen, J.A. Taylor, J. Vac. Sci. Technol. 21 (1982) 933.
[17] V.A. Beliy, K. Ludema, N.K. Mishkin, Tribology: Studies and Applications — USA and USSR Experience, Allerton Press, New York, 1993, p. 202.
[18] S. Kim, G.J. Kim, M.C. Kang, J.W. Kim, K.H. Kim, Surf. Coat. Technol. 193 (2005) 249.
[19] J.L. Endrino, V. Derflinger, Surf. Coat. Technol. 200 (2005) 988.
[20] W. Gao, Z. Liu, Z. Li, H. Gong, Appl. Phys. 16 (2002) 128.
[21] Y. Tanaka, N. Ichimiya, Y. Onishi, Y. Yamada, Surf. Coat. Technol. 146–147 (2001) 215.